Journal of Fluids and Structures 71 (2017) 70–77

Contents lists available at ScienceDirect

Journal of Fluids and Structures

journal homepage: www.elsevier.com/locate/yjfls

Hydrodynamic advantages of a low aspect-ratio flapping foil

Jeongsu Lee [a], Yong-Jai Park [b], Kyu-Jin Cho [a], Daegyoum Kim [c,*], Ho-Young Kim [a,d,*]

[a] Department of Mechanical and Aerospace Engineering, Seoul National University, Seoul 08826, Republic of Korea
[b] Department of Mechanical Engineering, Sunmoon University, Asan 31460, Republic of Korea
[c] Department of Mechanical Engineering, KAIST, Daejeon 34141, Republic of Korea
[d] Big Data Institute, Seoul National University, Seoul 08826, Republic of Korea

ARTICLE INFO

Article history:
Received 26 September 2016
Received in revised form 21 March 2017
Accepted 28 March 2017

Keywords:
Aquatic locomotion
Caudal fin
Vortical structure
Flapping
Propulsion

ABSTRACT

A high aspect-ratio foil is known to be advantageous in terms of both thrust and efficiency in flapping propulsion. However, many species of fish have evolved a low aspect-ratio hydrofoil, which naturally leads one to search for its physical advantages in locomotion. Here we study the flow physics of a hydrofoil in angular reciprocating motion with negligible free-stream velocity to reveal the effects of an aspect ratio on hydrodynamic performance. By establishing a scaling law for the thrust of a foil of general shapes and corroborating it experimentally, we find that the thrust of an angularly reciprocating foil is maximized at a low aspect ratio of 0.7 while hydromechanical efficiency continuously increases with an aspect ratio. This result suggests that a low aspect-ratio foil can improve thrust produced by the foil when they start from rest, but at the expense of efficiency.

1. Introduction

Most of swimming and flying animals flap their fins or wings to propel through a surrounding fluid. The topics of flapping locomotion that have been addressed thus far include measuring the precise kinematics of animals (Fish and Lauder, 2006; Shelton et al., 2006), analyzing the flow structure and forces of a flapping foil (von Ellenrieder et al., 2003; Dong et al., 2006; Buchholz and Smits, 2008; Green and Smits, 2008; Kim and Gharib, 2013) and examining the role of an aspect ratio and flexibility of fish-like locomotion (Dewey et al., 2013; Raspa et al., 2014; Feilch and Lauder, 2015; Quinn et al., 2015; Yeh and Alexeev, 2016). One of the important issues in the mechanics of flapping propulsion is the effect of an aspect ratio of the foil. Early studies have proposed that a high aspect-ratio foil is advantageous in terms of both thrust coefficient and hydromechanical efficiency (Chopra, 1974; Chopra and Kambe, 1977; Cheng and Murillo, 1984; Karpouzian et al., 1990; Dong et al., 2006; Buchholz and Smits, 2008; Green and Smits, 2008; Dewey et al., 2013).

However, many biological studies revealed clear distinction of the caudal fin aspect ratio between migratory and non-migratory fish (Nursall, 1958; Webb, 1984; Domenici and Blake, 1997; Flammang and Lauder, 2009; Domenici and Kapoor, 2010). The data on the aspect ratio are summarized in Fig. 1. The highly migratory fish, which are expected to give priority to efficiency improvement in cruising, have a high aspect-ratio caudal fin as shown in Fig. 1a. On the other hand, non-migratory fish generally have a smaller aspect ratio than migratory fish. The comparison in normalized coordinates in Fig. 1c,d clearly shows the stark difference of the caudal fin shape between migratory and non-migratory fish. We further compared the distribution of the caudal fin aspect ratio of highly migratory and non-migratory marine fish in Fig. 1e (refer

* Corresponding authors.
E-mail addresses: daegyoum@kaist.ac.kr (D. Kim), hyk@snu.ac.kr (H.-Y. Kim).

http://dx.doi.org/10.1016/j.jfluidstructs.2017.03.006

Table 1
Experimental parameters.

h	Height	1.5–22.5 cm
w	Width	1.2–20 cm
Λ	Sweepback angle	0–53 deg
l_s	Side length	0–20 cm
$2\theta_m$	Stroke angle	35 deg
f	Frequency	0.1–2.5 Hz
R	Radius of rotation	13.2–32 cm
S	Surface area	24–96 cm^2

to Supplementary Material for the definition of an aspect ratio and the data of the aspect ratio of aquatic animals). In general, the former group has a caudal fin of a high aspect ratio, whereas the latter has a caudal fin of a much smaller aspect ratio.

The comparative studies on the fish caudal fins of diverse species found that a high aspect ratio is advantageous for efficiency improvement in cruising while a low aspect ratio is advantageous for thrust maximization in sprinting (Nursall, 1958; Webb, 1984; Domenici and Blake, 1997; Flammang and Lauder, 2009; Domenici and Kapoor, 2010), which is inconsistent with the conventional hydrodynamic argument that a high aspect ratio is advantageous in terms of both thrust and efficiency (Chopra, 1974; Chopra and Kambe, 1977; Cheng and Murillo, 1984; Karpouzian et al., 1990; Dong et al., 2006; Buchholz and Smits, 2008; Green and Smits, 2008; Dewey et al., 2013). Such controversy has not been treated or resolved by fluid-dynamic theory thus far. In this study, we investigate physical mechanisms underlying the advantages of a low aspect-ratio foil and resolve the inconsistent views on the role of an aspect ratio on thrust and efficiency.

In this study, we investigate the hydrodynamics of a flapping foil without steady forward motion as an elementary model of the situation where the caudal fin is used to propel from rest and especially focus on the effects of an aspect ratio on thrust and efficiency. Despite extensive fluid dynamic studies on flapping locomotion, most of them have considered heaving and/or pitching of a foil in steady forward motion or against incoming freestream. The hydrodynamics of a flapping foil without steady forward motion has drawn relatively less scientific interest. The vortex formation around a flapping foil that rotates from rest without forward motion has been investigated recently (Ahlborn et al., 1997; Kim and Gharib, 2011; DeVoria and Ringuette, 2012). The theoretical model for the thrust of an angularly reciprocating rectangular plate has been suggested based on flow visualization (Lee et al., 2013). However, the effect of an aspect ratio on thrust and efficiency in such a motion has not been addressed by the previous studies.

2. Experimental apparatus

An angularly reciprocating foil as an elementary model of a flapping foil at the start of locomotion is shown in Fig. 2. The foil was immersed in a transparent water tank of 75, 55, and 33 cm in the x-, y- and z-directions, respectively. The foil is in a single degree-of-freedom sinusoidal oscillation about the z-axis, and the rotating axis is fixed in space. We employed rectangular, trapezoidal and cropped delta foils of various dimensions; the ranges of design dimensions are height $h = [1.5\ 22.5]$ cm, width $w = [1.2\ 20]$ cm, sweepback angle of quarter-chord line $\Lambda = [0\ 53]$ deg, and side length $l_s = [0\ 20]$ cm. The foil shape used in this study roughly mimics a caudal fin. The foil is attached to a metallic rod of length $l = 12$ cm which oscillates about the z-axis. The radius of rotation of the foil tip is $R = [13.2\ 32]$ cm. While a rotating axis is on the chord of a foil in usual pitching and/or heaving models, in our model, a rotating axis is outside the chord of a foil. The stroke angle of the sinusoidal rotation $2\theta_m$ is fixed to 35°. The flapping frequency f ranges from 0.1 to 2.5 Hz. The experimental parameters are summarized in Table 1. The Reynolds number Re is defined as $Re = Uw/\nu$ where U and ν are characteristic velocity and kinematic viscosity, respectively. In our experiments, the Reynolds number Re, based on the period-averaged speed at 0.7 radius length $U = 4(0.7R)\theta_m f$ (Techet, 2008), ranges from 1.3×10^3 to 1.1×10^5. The other dimensionless parameters are varied such that the aspect ratio $A = h^2/S = [0.075\ 17]$ where S is a surface area, the normalized stroke amplitude $\beta = 2R\theta_m/w = [0.9\ 6.7]$, the height-to-width ratio $\eta = h/w = [0.075\ 17]$, and the taper ratio $\lambda = l_s/w = [0\ 1]$.

The velocity and vorticity fields were obtained from two-dimensional Digital Particle Image Velocimetry (DPIV) using hydrogen bubbles as seeding particles. The hydrogen bubbles are generated by the electrolysis of water using a platinum wire of 50 − m. The electrical power applied to the platinum wire is controlled by a power supply (Kenex HV-401) to maintain the size of hydrogen bubbles similar to the diameter of the platinum wire. To visualize the bubbles, the central plane perpendicular to the flapping tail was illuminated using a 2 W continuous laser with a 532 nm wavelength. The captured images were analyzed using DPIV software to generate velocity fields with an interrogation window size of 32 × 32 pixels with a 50% overlap. The processed velocity vectors were validated using a dynamic mean value operator. The number of error vectors was within 2% of the total number of velocity vectors. The thrust generated by the foil in the y-axis was also measured by a miniature load cell (Kyoto 333FB) at a sampling rate of 2 kHz. The capacity of a load cell is 4.9 N, and the precision is 0.1%, corresponding to the accuracy of about 0.005 N.

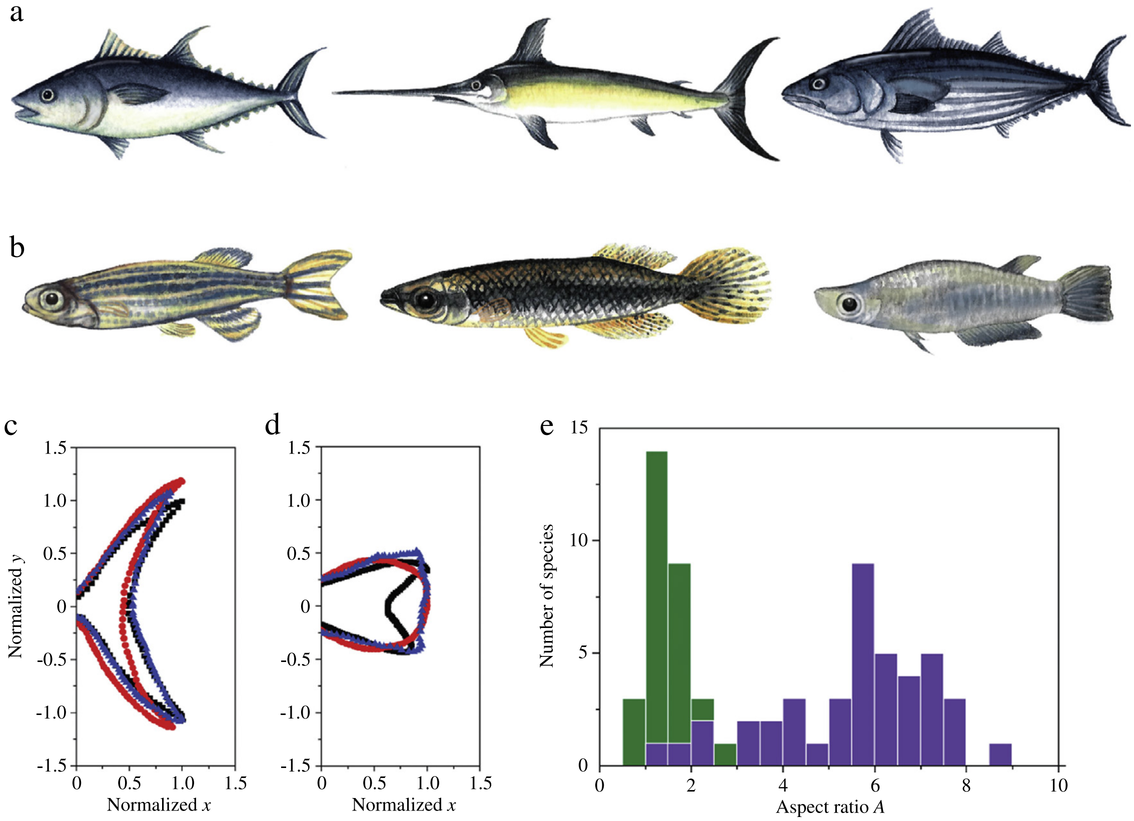

Fig. 1. (a) Highly migratory fish with a high aspect-ratio caudal fin. From left to right: tuna, swordfish and bonito. (b) Non-migratory fish with a low aspect-ratio caudal fin. From left to right: zebrafish, black stripe topminnow and rice fish. (c) The caudal fin profiles of highly migratory fish normalized by maximum length of the caudal fin: tuna (black), swordfish (red) and bonito (blue). (d) The caudal fin profiles of non-migratory fish normalized by maximum length of the caudal fin: zebrafish (black), stripe topminnow (red) and rice fish (blue). (e) Distribution of the aspect ratio of highly migratory marine fish (purple) and non-migratory marine fish (green). The aspect ratio A is defined as h^2/S where h is the maximum (tip to tip) span of the fin and S is the projected area of a fin planform. Also refer to Supplementary material. (For interpretation of the references to colour in this figure legend, the reader is referred to the web version of this article.)

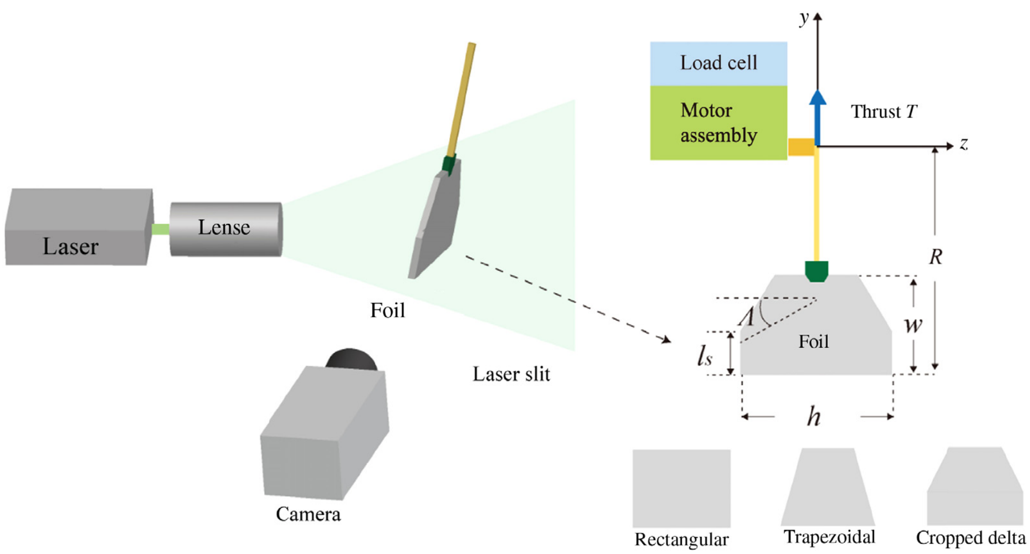

Fig. 2. Schematic illustration of the experimental apparatus.

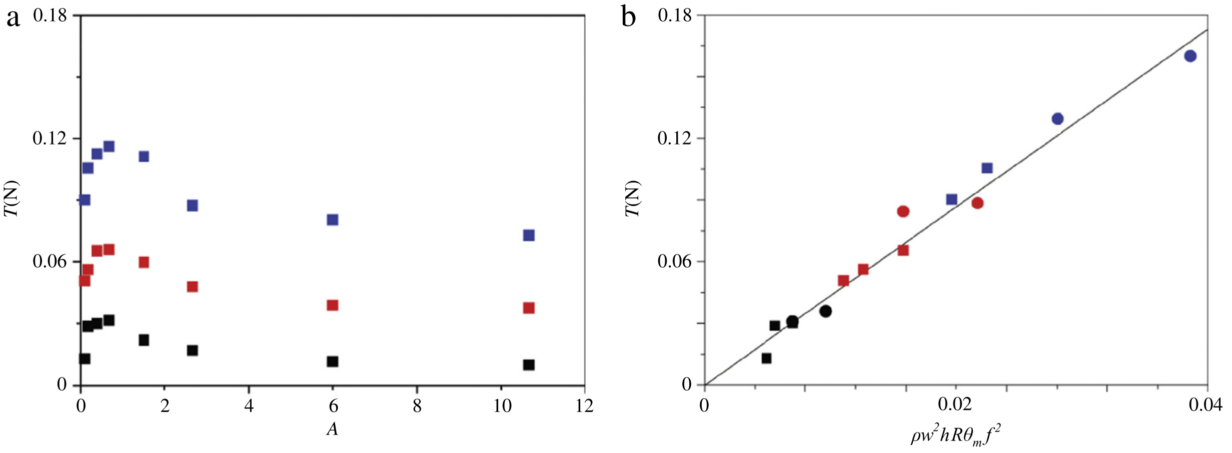

Fig. 3. (a) Thrust of a rectangular foil versus an aspect ratio. (b) Thrust below the slenderness limit versus $\rho h^2 wR\theta_m f^2$. A solid line is from the added-mass force theory. The black, red and blue symbols correspond to the frequency of $f = 1, 1.5, 2$ Hz, respectively. The squares and circles correspond to the rectangular foil with the area of 24 and 30 cm^2, respectively.

3. Results

3.1. Scaling law and added-mass theory

We first measured the thrust of a rectangular foil by varying an aspect ratio A over two orders of magnitude as shown in Fig. 3a. The trend in thrust curves changes at the aspect ratio of about 0.7. Before the transition, the thrust rapidly increases with the aspect ratio. However, after the transition, the thrust decreases gradually with the aspect ratio. For a slender foil with an extremely low aspect ratio, the hydrodynamic force can be modeled as an added-mass force based on the potential flow assumption (Lighthill, 1970; Ellington, 1984). The thrust is scaled as the product of the added mass $\sim\rho h^2 w$ and the acceleration $\sim R\theta_m f^2$:

$$T \sim \rho h^2 wR\theta_m f^2. \tag{1}$$

The thrust for an aspect ratio smaller than 0.7 is successfully predicted by (1), as shown in Fig. 3b, where thrust data measured experimentally collapse onto a straight line when plotted according to the scaling law (1). However, as the aspect ratio increases beyond the slenderness limit ($A \approx 0.7$), the added-mass theory based on the potential flow assumption is no longer valid since vortical structures generated by the foil should be taken into consideration.

3.2. Vortical structure of a flapping foil

In order to find the force production mechanism beyond the slenderness limit, we first identify the flow structures generated by a flapping foil as shown in Fig. 4a. The thrust of the angularly reciprocating foil is produced by the reaction of the momentum imparted to the vortical structures. When the foil accelerates to rotate, the vortical structures of an acceleration phase (APS: acceleration phase vortical structure) are formed at the edges of the foil (Fig. 4a(i–ii)). When the foil decelerates and reverses its direction, a strong vortical flow (SRV: stroke reversal vortical structure) is generated around the foil edges, as shown in Fig. 4a(iii–iv). The flapping foil, then, experiences thrust as shown in the sharp force peak around the stroke reversal of Fig. 4b, as reaction of the momentum imparted to the SRV. The SRV is shed away from the flapping foil immediately after the stroke reversal as shown in Fig. 4a(v). When the foil rotates after the stroke reversal, a second APV is generated by foil acceleration, as shown in Fig. 4a(v–vi). The momentum transfer through the generation of the APV is another source of thrust, as indicated by a second force peak in the time history of the thrust in Fig. 4b. The APV follows the motion of the foil until the next stroke reversal, and the vorticity separated at the foil edges continuously feed into the APV as shown in Fig. 4a(i–ii) and Fig. 4a(v–vi). Although not presented here, for all foil geometries considered in this study, SRV and APV were identified in flow visualization, and the peaks corresponding to SRV and APV were found in thrust curves.

We note that flapping frequency is different between Fig. 4a and b due to the limitation of our experimental apparatus. While the power of laser source limited PIV experiment to the flapping frequency below 0.2 Hz, force measurement for the flapping frequency below 0.5 Hz was not available due to basic noise level in our load cell. However, we suppose that this limitation in our experimental apparatus does not affect our arguments based on the observation that basic flow patterns –two distinct vortical structures per half cycle –does not change in a frequency range from 0.2 to 2 Hz.

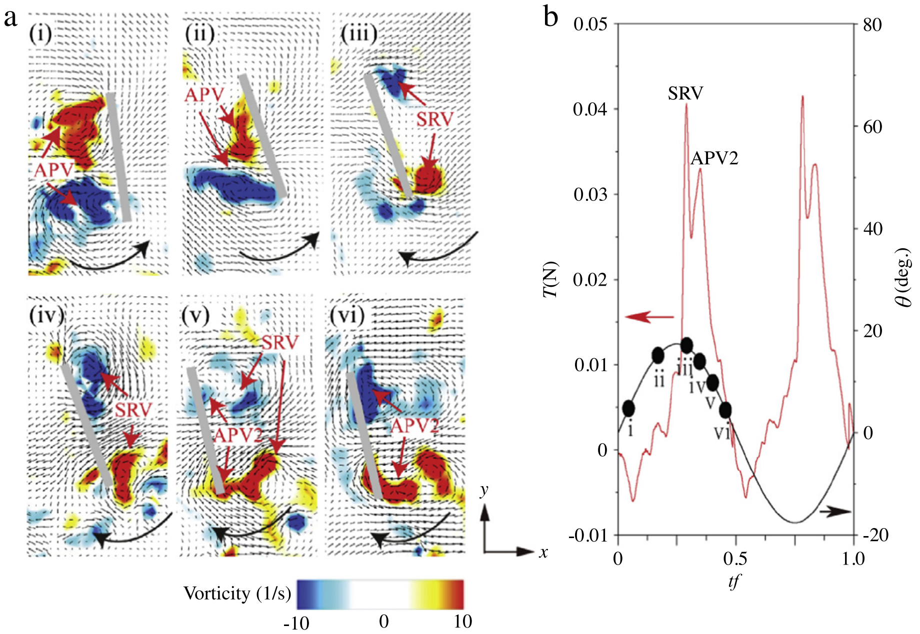

Fig. 4. (a) Velocity vectors and vorticity contours around a trapezoidal foil with $[h, w] = [4, 12]$ cm, oscillating at 0.2 Hz. (i)-(vi) correspond to dimensionless time $tf = 0.04$, 0.18, 0.29, 0.36, 0.43 and 0.46. Round arrows indicate the instantaneous rotating direction of the foil. Blue and red contours correspond to clockwise and counterclockwise vorticities, respectively. We denote a vortical structure in a counterclockwise stroke as APV, a vortical structure in a stroke reversal as SRV, and a vortical structure in a clockwise stroke as APV2. (b) Thrust of a trapezoidal foil with $[h, w] = [4, 12]$ cm, oscillating at 0.5 Hz. Black and red arrows indicate that the black and red curves correspond to stroke angle θ and thrust T, respectively. The times corresponding to (i)-(vi) of (a) are presented on the displacement curve of (b). (For interpretation of the references to colour in this figure legend, the reader is referred to the web version of this article.)

3.3. Scaling law and vortical structure

Based on the observed flow structures in Section 3.2, we construct a scaling law for the thrust of the foil of the aspect ratio larger than the slenderness limit ($A \approx 0.7$). The period-averaged thrust, T, is a function of fluid density and dynamic viscosity (ρ, μ), stroke frequency (f), stroke angle (θ_m), radius of rotation (R), foil dimensions (h, w), sweepback angle (Λ), and side length (l_s): $T = fn(\rho, \mu, R, h, w, f, \theta_m, \Lambda, l_s)$. Applying the Buckingham Pi theorem, one obtains the following dimensionless relationship:

$$\frac{T}{\rho w^4 f^2} = f(Re, A, \beta, \eta, \Lambda, \lambda), \tag{2}$$

where $Re = Uw/\nu$ is the Reynolds number, $A = h^2/S$ is the aspect ratio, $\beta = 2R\theta_m/w$ is the normalized stroke amplitude, $\eta = h/w$ is the height-to-width ratio, and $\lambda = l_s/w$ is the taper ratio.

The thrust is produced by reaction of the momentum imparted to the vortical structures, i.e., APV and SRV. The period-averaged thrust, T, can then be scaled as a product of the frequency, f, and the momentum imparted to the vortical structures per cycle, ΔI; $T \sim f\Delta I$. The momentum imparted to the fluid consists of two parts associated with the APV and SRV as $\Delta I \sim I_A + I_S$, where subscripts A and S denote APV and SRV, respectively. Vorticity is concentrated in a separated shear layer around the foil edges. Thus, the momentum induced by the vortical structure is modeled as $I_i \sim \rho\Gamma_i S$, where Γ_i is the circulation of the vortical structure, S is the area of the foil, and the subscript i is either A or S (Wu et al., 2006). The circulation Γ_i is scaled with the strength of the vortex at the bottom tip. Therefore, the period-averaged thrust can be expressed as $T \sim (I_A + I_S)f \sim \rho(\Gamma_A + \Gamma_S)Sf$.

The scaling relation for Γ_i is obtained by applying the following physical constraint. The pressure difference across the front and back surfaces should be zero at the bottom tip of the foil where a vortex sheet is separated into the flow field (Theodorsen, 1935; Wu et al., 2006). Two distinct effects inducing the pressure difference at the tip should counterbalance each other: one is the acceleration of the foil, and another is the tangential velocity discontinuity induced by the vortex sheet (Theodorsen, 1935; Wu et al., 2006). This physical constraint allows us to write $\Delta p_a \sim \rho(\Delta U_t)^2$, where Δp_a is pressure difference induced by the acceleration and ΔU_t is tangential velocity difference between the front and back surfaces at the tip.

The acceleration of the foil a varies along the width-wise direction, whereas it is a constant along the height-wise direction. Therefore, the pressure difference at the tip induced by acceleration, Δp_a, can be scaled using the added mass force of the blade element with a width Δw and a height h, $F_a \sim \rho h^2 \Delta w a$. The pressure difference is then scaled as $\Delta p_a \sim F_a/(\Delta w h) \sim \rho h a$. Next, the tangential velocity discontinuity, ΔU_t, can be related to the strength of the vortex at the bottom tip as $\Delta U_t \sim \Gamma_i/w$ because the vortex sheet on the foil surface is separated tangentially and evolves into a tip vortex at the foil tip. Therefore, the characteristic circulation is expressed as $\Gamma_i \sim w h^{1/2} a_i^{1/2}$. Here the subscript i of acceleration a and circulation Γ is A for APV and S for SRV. Assuming that the motion of the foil follows a simple harmonic function in time, the deceleration and acceleration of the foil can be scaled as $a_A \sim a_S \sim R\theta_m f^2$, where $R\theta_m$ is the distance traveled by the foil tip. Then, the characteristic circulation can be also scaled as a single expression, $\Gamma_A \sim \Gamma_S \sim w h^{1/2} R^{1/2} \theta_m^{1/2} f$. Finally substituting this scaling for the circulation into the scaling law for the thrust $T \sim \rho(\Gamma_A + \Gamma_S)Sf$, the thrust is given by

$$T \sim \rho S w h^{1/2} R^{1/2} \theta_m^{1/2} f^2. \tag{3}$$

In order to validate our scaling law, we collected thrust data of 195 cases by varying foil dimensions, flapping frequency, stroke amplitude, and foil shapes, and compared them with relation (3). As shown in Fig. 5b, all thrust data collapse onto a straight line when plotted according to (3). Meanwhile, the data are scattered when plotted versus $\rho S R^2 \theta_m^2 f^2$ in Fig. 5a, which corresponds to the conventional scaling of hydrodynamic force $\rho U^2 S$ with $U \sim R\theta_m f$. We further examine the dimensionless relation of the thrust by dividing both sides of (3) with $\rho w^4 f^2$:

$$\frac{T}{\rho w^4 f^2} \sim \frac{\eta^{5/2} \beta^{1/2}}{A}. \tag{4}$$

The dimensionless thrust is a function of the height-to-width ratio η, the normalized stroke amplitude β, and the aspect ratio A, but is independent of the Reynolds number Re, the sweepback angle Λ, and the taper ratio λ. In the range of Re studied in this work, our dimensionless scaling law is in good agreement with the experimental measurements, as shown in Fig. 5c.

3.4. Optimal aspect ratio

Based on the scaling law, we investigate the effects of the aspect ratio on thrust and efficiency. We note that (3) can be rearranged as

$$\tilde{T} = \frac{T}{\rho (R\theta_m)^{1/2} S^{7/4} f^2} \sim A^{-1/4}. \tag{5}$$

In other words, the scaled thrust, $\tilde{T}$, is dependent on only A for the given stroke amplitude $R\theta_m$, foil area S, and frequency f. The scaled values of experimentally measured thrust, $\tilde{T}$, is plotted versus A in Fig. 6a. The trend in the thrust curve is abruptly changed at the slenderness limit, the aspect ratio of approximately 0.7. Before the transition, the thrust rapidly increases with the aspect ratio A, as predicted by the scaling law (1). However, beyond the slenderness limit, the thrust decreases with the aspect ratio, $\tilde{T} \sim A^{-1/4}$, as predicted by the scaling law (5). Therefore, the aspect ratio around the slenderness limit, $A \approx 0.7$ is optimal in maximizing the thrust for the given foil area and kinematics.

We next examine the relationship between an aspect ratio and efficiency. In general, the hydromechanical efficiency of a flapping foil is defined as a ratio of the work used for propulsion to the total work conducted through foil motion, i.e., the Froude efficiency (Lighthill, 1970; Sfakiotakis et al., 1999). However, the efficiency of our foil model cannot be obtained using the conventional definition because the work used for propulsion is zero owing to the absence of forward motion. Instead, we introduce the hydrodynamic cost of endurance as a measure of efficiency, which is analogous to the aerodynamic cost of endurance in hovering insects (Wang, 2008; Lentink and Dickinson, 2009; Pesavento and Wang, 2009). The hydrodynamic cost of endurance C is defined as a dimensionless power to produce a unit thrust, $C = Wf/(TU_r)$, where W is the work conducted by the tail motion defined as $W = \int_0^{1/f} \tau \cdot \Omega dt$ with torque τ and angular velocity Ω. The reference velocity $U_r = \sqrt{2T/(\rho S)}$ is constant for a given tail area S and thrust T. The inverse of the hydrodynamic cost of endurance can be considered as the efficiency of the angularly reciprocating tail.

The scaling law for C can be obtained using the scaling relation for the thrust (3). For the work conducted by the foil motion: $W \sim TR\theta_m \sim \rho S w h^{1/2} R^{3/2} \theta_m^{3/2} f^2$, we get

$$C \sim \frac{R\theta_m}{w} A^{-1/4} \sim \beta A^{-1/4}. \tag{6}$$

The ratio of C to β is plotted versus the aspect ratio in Fig. 6b. The hydrodynamic cost of endurance decreases rapidly with the aspect ratio up to the slenderness limit, implying a drastic improvement in efficiency. The decreasing trend in the hydrodynamic cost of endurance with A weakens after the slenderness limit. C/β scales with $A^{-1/4}$ after the slenderness limit as predicted by the scaling law (6).

4. Discussion

From the experiment and modeling for thrust and efficiency, we are able to infer the following guidelines to determine the aspect ratio maximizing the propulsive performance at the start of locomotion. First, an aspect ratio below the slenderness

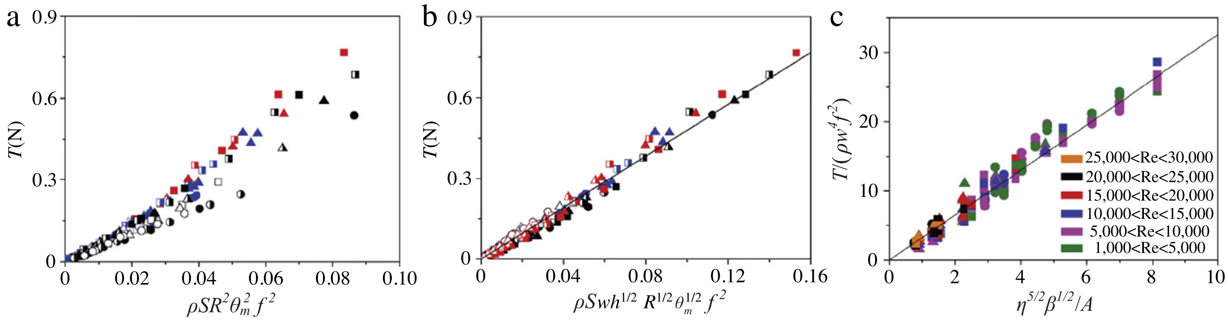

Fig. 5. Scaling relations of period-averaged thrust. (a, b) Plots of period-averaged thrust versus $\rho SR^2\theta_m^2 f^2$ and the scaling law (3), respectively, for various foil dimensions and shapes. Black, red, and blue symbols correspond to the rectangular, trapezoidal, and cropped delta foils, respectively. Circles, triangles, and squares correspond to foils of $w = 6$, 9, and 12 cm, respectively. Empty, half-filled, and filled symbols correspond to foils of $h = 4$, 6, and 8 cm, respectively. (c) Dimensionless thrust, $T/(\rho w^4 f^2)$, versus $\eta^{5/2}\beta^{1/2}/A$ for various foil dimensions and shapes. Circles, triangles, and squares correspond to the cropped delta, trapezoidal, and rectangular foils, respectively. (For interpretation of the references to colour in this figure legend, the reader is referred to the web version of this article.)

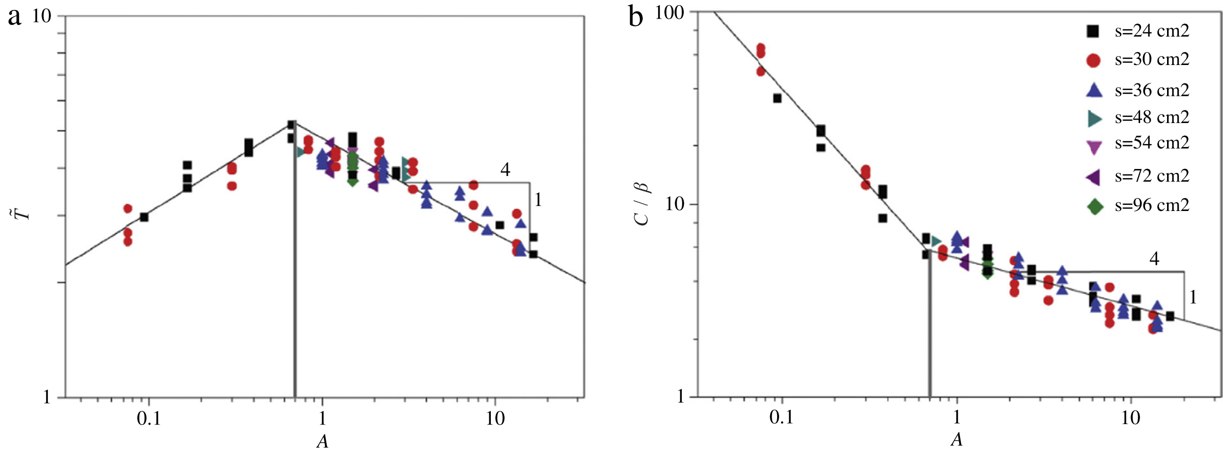

Fig. 6. Effects of an aspect ratio, A, on thrust and efficiency. (a) Scaled thrust, $\tilde{T} = T/\rho(R\theta_m)^{1/2}S^{7/4}f^2$, of Eq. (5) versus an aspect ratio. (b) The ratio of hydrodynamic cost of endurance to normalized stroke amplitude, C/β, versus an aspect ratio. The vertical lines in (a) and (b) indicate the slenderness limit ($A \approx 0.7$). Squares, circles, triangles, right-pointing triangles, down-pointing triangles, left-pointing triangles, and diamonds correspond to the rectangular foils with the area of 24, 30, 36, 48, 54, 72 and 96 cm^2, respectively.

limit ($\approx$ 0.7) should be avoided because it is unfavorable in terms of both thrust and efficiency. Second, for the purpose of thrust maximization, the aspect ratio around the slenderness limit, i.e., $\approx$ 0.7, is preferred. On the other hand, the efficiency is continuously improved as the aspect ratio increases, although there is a loss in thrust above the slenderness limit. Maximizing the aspect ratio within the limitation of structural requirements is advantageous for the purpose of improving the efficiency. Therefore, the optimal aspect ratio of a propulsive system is determined by considering a tradeoff between thrust and efficiency whose relations to the aspect ratio are given in the scaling laws (5) and (6).

In order to examine whether our results favorably correspond to biological observations of actual fish, we further examine the caudal fin aspect ratio of non-migratory fish (data in Supplementary Material). The non-migratory fish is expected to have a higher priority on thrust maximization at the start of locomotion for immediate escape response from a predator. Only 2% of non-migratory fish are distributed within the aspect ratio below the slenderness limit ($\approx$ 0.7), which is shown to be disadvantageous in terms of both hydrodynamic thrust and efficiency in our study. Majority of the non-migratory fish ($\sim$ 51%) are distributed within the aspect ratio ranging from 0.7 to 1.5. While $A = 0.7$ corresponds to the slenderness limit that maximizes the thrust with given tail area and kinematics, at $A = 1.5$ the efficiency is expected to improve by about 17% despite a loss in thrust by 17% compared to the values at the slenderness limit. Furthermore, most of the non-migratory fish ($\sim$ 79%) have the aspect-ratio smaller than 2. The trends in aspect ratio distribution show that non-migratory fish adopt following two strategies; 1) an aspect ratio below the slenderness limit is avoided, 2) a considerable number of non-migratory fish tune the aspect ratio of the caudal fin to be slightly above the slenderness limit. These results suggest that a large number of non-migratory fish species have selected a low-to-moderate aspect ratio fin by the tradeoff between thrust and efficiency at the start of locomotion.

5. Conclusion

In this study, by using scaling arguments for added-mass force and vortical impulse, we addressed a novel mechanism to explain the hydrodynamic advantage of a low aspect-ratio foil, which resolves the inconsistency of biological observations and conventional fluid dynamic viewpoints. The efficiency continuously improves as the aspect ratio increases, although there is a loss in thrust above the slenderness limit. On the other hand, for the purpose of thrust maximization, the aspect ratio around the slenderness limit, $A \approx 0.7$, is desirable. The aspect ratio below the slenderness limit is unfavorable in terms of both thrust and efficiency. For the start of locomotion, a low aspect-ratio foil near the slenderness limit can maximize thrust. Therefore, a low aspect-ratio foil, near the slenderness limit, can be a better choice than a high aspect-ratio foil for the situations where thrust generation for fast response from rest is crucial such as an escape from a predator (Domenici and Blake, 1997).

Acknowledgments

This research was supported by National Research Foundation of Korea (Grant Nos. 2015R1C1A1A02037111, 2016901290 and 2016913167) and administered via SNU IAMD.

Appendix A. Supplementary data

Supplementary material related to this article can be found online at http://dx.doi.org/10.1016/j.jfluidstructs.2017.03.006.

References

Ahlborn, B., Chapman, S., Stafford, R., Blake, R.W., Harper, D.G., 1997. Experimental simulation of the thrust phases of fast-start swimming of fish. J. Exp. Biol. 200, 2301–2312.
Buchholz, J.H.J., Smits, A.J., 2008. The wake structure and thrust performance of a rigid low-aspect-ratio pitching panel. J. Fluid Mech. 603, 331–365.
Cheng, H.K, Murillo, L.E, 1984. Lunate-tail swimming propulsion as a problem of curved lifting line in unsteady flow. Part 1. Asymptotic theory. J. Fluid Mech. 143, 327–350.
Chopra, M.G., 1974. Hydromechanics of lunate-tail swimming propulsion. J. Fluid Mech. 64, 375–392.
Chopra, M.G, Kambe, T., 1977. Hydromechanics of lunate-tail swimming propulsion. Part 2. J. Fluid Mech. 79, 49–69.
Ellington, C.P., 1984. The aerodynamics of hovering insect flight. I. The quasi-steady analysis. Phil. Trans. R. Soc. Lond. B 305, 1–15.
DeVoria, A.C., Ringuette, M.J., 2012. Vortex formation and saturation for low-aspect-ratio rotating flat-plate fins. Exp. Fluids 52, 441–462.
Dewey, P.A., Boschitsch, B.M., Moored, K.W., Stone, H.A., Smits, A.J., 2013. Scaling laws for the thrust production of flexible pitching panels. J. Fluid Mech. 732, 29–46.
Domenici, P., Blake, R., 1997. The kinematics and performance of fish fast-start swimming. J Exp. Biol. 200, 1165–1178.
Domenici, P., Kapoor, B.G, 2010. Fish Locomotion: An Eco-Ethological Perspective. Enfield. Science Publishers.
Dong, H., Mittal, R., Najjar, F.M., 2006. Wake topology and hydrodynamic performance of low-aspect-ratio flapping foils. J. Fluid Mech. 566, 309–343.
Feilch, K.L., Lauder, G.V., 2015. Passive mechanical models of fish caudal fins: effects of shape and stiffness on self-propulsion. Bioinspir. Biomim. 10, 036002.
Fish, F.E., Lauder, G.V., 2006. Passive and active flow control by swimming fishes and mammals. Annu. Rev. Fluid Mech. 38, 193–224.
Flammang, B.E., Lauder, G.V., 2009. Caudal fin shape modulation and control during acceleration, braking and backing maneuvers in bluegill sunfish, lepomis macrochirus. J. Exp. Biol. 212, 277–286.
Green, M.A., Smits, A.J., 2008. Effects of three-dimensionality on thrust production by a pitching panel. J. Fluid Mech. 615, 211–220.
Karpouzian, G., Spedding, G., Cheng, H.K, 1990. Lunate-tail swimming propulsion. Part 2. Performance analysis. J. Fluid Mech. 210, 329–351.
Kim, D., Gharib, M., 2011. Characteristics of vortex formation and thrust performance in drag-based paddling propulsion. J. Exp. Biol. 214, 2283–2291.
Kim, D., Gharib, M., 2013. Vortex dynamics of clapping plates. J. Fluid Mech. 714, 5–23.
Lee, J., Park, Y.-J., Jeong, U., Cho, K.-J., Kim, H.-Y., 2013. Wake and thrust of an angularly reciprocating plate. J. Fluid Mech. 720, 545–557.
Lentink, D., Dickinson, M.H., 2009. Rotational accelerations stabilize leading edge vortices on revolving fly wings. J. Exp. Biol. 212, 2705–2719.
Lighthill, M.J., 1970. Aquatic animal propulsion of high hydromechanical efficiency. J. Fluid Mech. 44, 265–310.
Nursall, J.R., 1958. The caudal fin as a hydrofoil. Evolution 12, 116–120.
Pesavento, U., Wang, Z.J, 2009. Flapping wing flight can save aerodynamic power compared to steady flight. Phys. Rev. Lett. 103, 118202.
Quinn, D.B., Lauder, G.V., Smits, A.J., 2015. Maximizing the efficiency of a flexible propulsor using experimental optimization. J. Fluid Mech. 767, 430–448.
Raspa, V., Ramananarivo, S., Thiria, B., Godoy-Diana, R., 2014. Vortex-induced drag and the role of aspect ratio in undulatory swimmers. Phys. Fluids 26, 041701.
Sfakiotakis, M., Lane, D.M., Davies, J.B.C., 1999. Review of fish swimming modes for aquatic locomotion. J. Ocean. Eng. 24, 237–252.
Shelton, R.M, Thornycroft, P.J.M, Lauder, G.V, 2006. Undulatory locomotion of flexible foils as biomimetic models for understanding fish propulsion. J. Exp. Biol. 217, 2110–2120.
Techet, A.H., 2008. Propulsive performance of biologically inspired flapping foils at high Reynolds numbers. J. Exp. Biol. 211, 274–279.
Theodorsen, T., 1935. General theory of aerodynamic instability and the mechanism of flutter. NACA Report 496.
von Ellenrieder, K.D., Parker, K., Soria, J., 2003. Flow structures behind a heaving and pitching finite-span wing. J. Fluid Mech. 490, 129–138.
Wang, Z.J., 2008. Aerodynamic efficiency of flapping flight: analysis of a two-stroke model. J. Exp. Biol. 211, 234–238.
Webb, P.W., 1984. Body form, locomotion and foraging in aquatic vertebrates. Am. Zool. 24, 107–120.
Wu, J.-Z., Ma, H.-Y., Zhou, M.-D., 2006. Vorticity and Vortex Dynamics. Springer, Berlin.
Yeh, P.D., Alexeev, A., 2016. Effect of aspect ratio in free-swimming plunging flexible plates. Comput. Fluids 124, 220–225.

Supplementary Material for “Hydrodynamic advantages of a low aspect-ratio flapping foil”

The data of the aspect ratio of fish species used in this study are listed in Tables S1-S3. All data were obtained from morphometric data of FishBase (http://www.fishbase.org) from January to June of 2015. The definition of the caudal fin aspect ratio *A* is shown in Fig. S1. Here *h* is the maximum (tip to tip) span of the fin and *S* is the projected area of a fin planform for a fish without any movement. In the table, we have highlighted the species used as a reference in the main text.

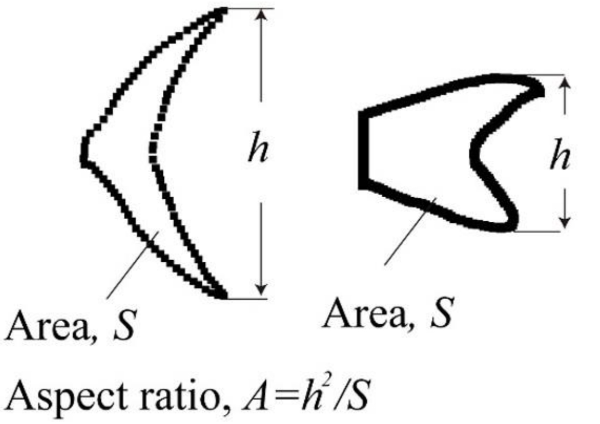

Fig. S1: Definition of the caudal fin aspect ratio.

Table. S1 Aspect ratio data of non-migratory marine fish

Common Name	*Species*	AR	Ref
Green damselfish	*Abudefduf abdominalis*	2.6	http://fishbase.org
Redmouth grouper	*Aethaloperca rogaa*	1.6	http://fishbase.org
Redmouth grouper	*Aethaloperca rogaa*	1.2	http://fishbase.org
Redmouth grouper	*Aethaloperca rogaa*	1.5	http://fishbase.org
Redmouth grouper	*Aethaloperca rogaa*	1.8	http://fishbase.org

Mutton hamlet	*Alphestes afer*	1.1	http://fishbase.org
Mutton hamlet	*Alphestes afer*	1.0	http://fishbase.org
Mutton hamlet	*Alphestes afer*	1.1	http://fishbase.org
Mutton hamlet	*Alphestes afer*	1.0	http://fishbase.org
Batuna damsel	*Amblyglyphidodon batunai*	1.1	http://fishbase.org
New Guinean frogfish	*Antennatus dorehensis*	0.9	http://fishbase.org
Slender grouper	*Anyperodon leucogrammicus*	1.4	http://fishbase.org
Atlantic needlefish	*Atlantic needlefish*	1.3	http://fishbase.org
Goldribbon soapfish	*Aulacocephalus temminckii*	1.3	http://fishbase.org
Goldribbon soapfish	*Aulacocephalus temminckii*	1.2	http://fishbase.org
Tailface sleeper	*Calumia godeffroyi*	0.8	http://fishbase.org
Peacock hind	*Cephalopholis argus*	1.5	http://fishbase.org
Peacock hind	*Cephalopholis argus*	1.4	http://fishbase.org
Peacock hind	*Cephalopholis argus*	1.4	http://fishbase.org
Chocolate hind	*Cephalopholis boenak*	1.4	http://fishbase.org
Chocolate hind	*Cephalopholis boenak*	1.4	http://fishbase.org
Chocolate hind	*Cephalopholis boenak*	1.4	http://fishbase.org
Chocolate hind	*Cephalopholis boenak*	1.3	http://fishbase.org
Graysby	*Cephalopholis cruentata*	1.3	http://fishbase.org
Graysby	*Cephalopholis cruentata*	3.6	http://fishbase.org
Bluespotted hind	*Cephalopholis cyanostigma*	1.4	http://fishbase.org
Bluespotted hind	*Cephalopholis cyanostigma*	1.5	http://fishbase.org
Bluelined hind	*Cephalopholis formosa*	1.5	http://fishbase.org
Bluelined hind	*Cephalopholis formosa*	1.4	http://fishbase.org
Bluelined hind	*Cephalopholis formosa*	1.5	http://fishbase.org
Bluelined hind	*Cephalopholis formosa*	1.2	http://fishbase.org
Coney	*Cephalopholis fulva*	1.2	http://fishbase.org
Coney	*Cephalopholis fulva*	1.5	http://fishbase.org
Coney	*Cephalopholis fulva*	1.2	http://fishbase.org
Leopard hind	*Cephalopholis leopardus*	1.6	http://fishbase.org
Leopard hind	*Cephalopholis leopardus*	1.8	http://fishbase.org
Leopard hind	*Cephalopholis leopardus*	1.2	http://fishbase.org
Coral hind	*Cephalopholis miniata*	1.5	http://fishbase.org
Coral hind	*Cephalopholis miniata*	1.8	http://fishbase.org
Coral hind	*Cephalopholis miniata*	1.6	http://fishbase.org
Coral hind	*Cephalopholis miniata*	1.6	http://fishbase.org
Tomato hind	*Cephalopholis sonnerati*	2.0	http://fishbase.org
Brownspotted grouper	*Epinephelus chlorostigma*	1.4	http://fishbase.org

Brownspotted grouper	*Epinephelus chlorostigma*	1.7	http://fishbase.org
Brownspotted grouper	*Epinephelus chlorostigma*	1.8	http://fishbase.org
Striped large-eye bream	*Gnathodentex aureolineatus*	2.6	http://fishbase.org
Striped large-eye bream	*Gnathodentex aureolineatus*	1.4	http://fishbase.org
Trumpet emperor	*Lethrinus miniatus*	2.2	http://fishbase.org
Trumpet emperor	*Lethrinus miniatus*	2.1	http://fishbase.org
Yellow-edged lyretail	*Variola louti*	1.5	http://fishbase.org
Yellow-edged lyretail	*Variola louti*	2.7	http://fishbase.org
Garish hind	*Cephalopholis igarashiensis*	1.5	http://fishbase.org
Garish hind	*Cephalopholis igarashiensis*	2.4	http://fishbase.org
Spotted weakfish	*Cynoscion nebulosus*	1.4	http://fishbase.org
Spotted weakfish	*Cynoscion nebulosus*	1.6	http://fishbase.org
Whitebait smelt	*Allosmerus elongatus*	1.1	http://fishbase.org
Glacier lantern fish	*Benthosema glaciale*	1.0	http://fishbase.org
Smallscale codlet	*Bregmaceros nectabanus*	1.1	http://fishbase.org
Spothead lantern fish	*Diaphus metopoclampus*	1.8	http://fishbase.org
California killifish	*Fundulus parvipinnis*	1.2	http://fishbase.org
Bayou killifish	*Fundulus pulvereus*	1.3	http://fishbase.org

Table. S2 Aspect ratio data of non-migratory freshwater fish

Common Name	***Species***	**AR**	**Ref**
-	*Alfaro huberi*	1.8	http://fishbase.org
Foureyes	*Anableps microlepis*	0.5	http://fishbase.org
-	*Aphanius apodus*	2.0	http://fishbase.org
Scaleless killifish	*Aphanius asquamatus*	1.7	http://fishbase.org
-	*Aphanius danfordii*	1.8	http://fishbase.org
-	*Aphanius dispar richardsoni*	1.4	http://fishbase.org
South european toothcarp	*Aphanius fasciatus*	1.1	http://fishbase.org
Spanish toothcarp	*Aphanius iberus*	1.6	http://fishbase.org
-	*Aphanius mento*	1.8	http://fishbase.org
-	*Aphanius sirhani*	1.6	http://fishbase.org
-	*Aphanius vladykovi*	1.2	http://fishbase.org
-	*Aphyosemion abacinum*	0.4	http://fishbase.org
Golden killi	*Aphyosemion aureum*	1.4	http://fishbase.org
Lyretail panchax	*Aphyosemion australe*	0.7	http://fishbase.org

Bamileke killi	*Aphyosemion bamilekorum*	1.0	http://fishbase.org
Bates' killi	*Aphyosemion batesii*	0.8	http://fishbase.org
Sky-blue killi	*Aphyosemion coeleste*	0.8	http://fishbase.org
Mbam killi	*Aphyosemion dargei*	1.1	http://fishbase.org
False jewel killi	*Aphyosemion exigoideum*	2.4	http://fishbase.org
Jewel killi	*Aphyosemion exiguum*	1.3	http://fishbase.org
-	*Aphyosemion fulgens*	1.0	http://fishbase.org
Gabon killi	*Aphyosemion gabunense*	1.5	http://fishbase.org
Herzog's killi	*Aphyosemion herzogi*	0.9	http://fishbase.org
-	*Aphyosemion primigenium*	1.5	http://fishbase.org
-	*Aphyosemion zygaima*	2.0	http://fishbase.org
Black lampeye	*Aplocheilichthys antinorii*	1.9	http://fishbase.org
Bukoba lampeye	*Aplocheilichthys bukobanus*	1.4	http://fishbase.org
Lake Rukwa lampeye	*Aplocheilichthys fuelleborni*	0.9	http://fishbase.org
Meshscaled topminnow	*Aplocheilichthys hutereaui*	1.1	http://fishbase.org
Johnston's topminnow	*Aplocheilichthys johnstoni*	0.8	http://fishbase.org
Striped topminnow	*Aplocheilichthys katangae*	0.8	http://fishbase.org
Big tailed lampeye	*Aplocheilichthys macrurus*	1.1	http://fishbase.org
Natal topminnow	*Aplocheilichthys myaposae*	1.0	http://fishbase.org
Tanganyika lampeye	*Aplocheilichthys pumilus*	1.2	http://fishbase.org
Bitschumbi lampeye	*Aplocheilichthys vitschumbaensis*	1.1	http://fishbase.org
-	*Aplocheilus kirchmayeri*	1.1	http://fishbase.org
Striped panchax	*Aplocheilus lineatus*	0.8	http://fishbase.org
Blue panchax	*Aplocheilus panchax*	0.9	http://fishbase.org
Dwarf panchax	*Aplocheilus parvus*	1.0	http://fishbase.org
-	*Barbus tyberinus*	1.3	http://fishbase.org
Top minnow	*Belonesox belizanus*	2.0	http://fishbase.org
-	*Brachyrhaphis cascajalensis*	0.7	http://fishbase.org
-	*Brachyrhaphis episcopi*	1.6	http://fishbase.org
Soconusco gambusia	*Brachyrhaphis hartwegi*	1.8	http://fishbase.org
-	*Brachyrhaphis hessfeldi*	2.1	http://fishbase.org
-	*Brachyrhaphis roseni*	1.5	http://fishbase.org
Champoton gambusia	*Carlhubbsia kidderi*	1.6	http://fishbase.org
Barred livebearer	*Carlhubbsia stuarti*	1.7	http://fishbase.org
Luther's spiny loach	*Cobitis lutheri*	1.0	http://fishbase.org
Railroad Valley springfish	*Crenichthys nevadae*	1.7	http://fishbase.org
Checkered pupfish	*Cualac tessellatus*	1.4	http://fishbase.org
Potosi pupfish	*Cyprinodon alvarezi*	1.5	http://fishbase.org

Cuatro Cienegas pupfish	*Cyprinodon bifasciatus*	1.3	http://fishbase.org
Devils Hole pupfish	*Cyprinodon diabolis*	1.4	http://fishbase.org
Carbonera pupfish	*Cyprinodon fontinalis*	1.2	http://fishbase.org
La Palma pupfish	*Cyprinodon longidorsalis*	2.5	http://fishbase.org
Pecos pupfish	*Cyprinodon pecosensis*	0.5	http://fishbase.org
Charco Palma pupfish	*Cyprinodon veronicae*	1.2	http://fishbase.org
Zebra danio	*Danio rerio*	1.3	http://fishbase.org
Barred danio	*Devario pathirana*	1.9	http://fishbase.org
Banded panchax	*Epiplatys annulatus*	0.7	http://fishbase.org
-	*Epiplatys chevalieri*	1.1	http://fishbase.org
Redspotted panchax	*Epiplatys lamottei*	0.8	http://fishbase.org
Grass pickerel	*Esox americanus vermiculatus*	1.1	http://fishbase.org
Muskellunge	*Esox masquinongy*	2.3	http://fishbase.org
Chain pickerel	*Esox niger*	2.3	http://fishbase.org
Amiet's Lyretail	*Fundulopanchax amieti*	0.6	http://fishbase.org
Arnold's killi	*Fundulopanchax arnoldi*	1.7	http://fishbase.org
Mamfe killi	*Fundulopanchax mamfensis*	1.3	http://fishbase.org
-	*Fundulopanchax scheeli*	0.8	http://fishbase.org
-	*Fundulopanchax spoorenbergi*	0.9	http://fishbase.org
Western starhead topminnow	*Fundulus blairae*	0.8	http://fishbase.org
Northern studfish	*Fundulus catenatus*	1.6	http://fishbase.org
Golden topminnow	*Fundulus chrysotus*	1.1	http://fishbase.org
Banded topminnow	*Fundulus cingulatus*	0.9	http://fishbase.org
Banded killifish	*Fundulus diaphanus*	0.8	http://fishbase.org
Starhead topminnow	*Fundulus dispar*	1.4	http://fishbase.org
Russetfin topminnow	*Fundulus escambiae*	0.6	http://fishbase.org
Mummichog	*Fundulus heteroclitus*	0.9	http://fishbase.org
Blackstripe topminnow	*Fundulus notatus*	0.8	http://fishbase.org
Blackspotted topminnow	*Fundulus olivaceus*	0.8	http://fishbase.org
Speckled killifish	*Fundulus rathbuni*	1.4	http://fishbase.org
Plains topminnow	*Fundulus sciadicus*	0.6	http://fishbase.org
Plains killifish	*Fundulus zebrinus*	1.3	http://fishbase.org
Yellowfin gambusia	*Gambusia alvarezi*	2.2	http://fishbase.org
Big Bend gambusia	*Gambusia gaigei*	0.9	http://fishbase.org
Crescent gambusia	*Gambusia hurtadoi*	1.7	http://fishbase.org
Striped gambusia	*Gambusia melapleura*	1.4	http://fishbase.org
Pecos gambusia	*Gambusia nobilis*	0.9	http://fishbase.org

Cuban gambusia	*Gambusia punctata*	1.9	http://fishbase.org
Mangrove gambusia	*Gambusia rhizophorae*	1.0	http://fishbase.org
Yucatan gambusia	*Gambusia yucatana*	2.1	http://fishbase.org
Goldbelly topminnow	*Girardinus falcatus*	1.8	http://fishbase.org
Metallic livebearer	*Girardinus metallicus*	1.4	http://fishbase.org
-	*Iksookimia hugowolfeldi*	1.0	http://fishbase.org
-	*Iksookimia koreensis*	1.0	http://fishbase.org
-	*Iksookimia longicorpa*	0.8	http://fishbase.org
Puan spine loach	*Iksookimia pumila*	1.2	http://fishbase.org
-	*Iksookimia yongdokensis*	0.9	http://fishbase.org
Flagfish	*Jordanella floridae*	2.1	http://fishbase.org
Mangrove rivulus	*Kryptolebias marmoratus*	0.8	http://fishbase.org
Saisi lampeye	*Lacustricola matthesi*	1.0	http://fishbase.org
-	*Lacustricola mediolateralis*	0.9	http://fishbase.org
-	*Lacustricola nigrolateralis*	0.9	http://fishbase.org
Tanganyika killifish	*Lamprichthys tanganicanus*	1.7	http://fishbase.org
-	*Lepidocephalichthys birmanicus*	0.8	http://fishbase.org
Pygmy killifish	*Leptolucania ommata*	1.1	http://fishbase.org
Cuban limia	*Limia vittata*	1.8	http://fishbase.org
Lake Tanganyika sardine	*Limnothrissa miodon*	1.6	http://fishbase.org
-	*Luciobarbus graellsii*	1.4	http://fishbase.org
Trout cod	*Maccullochella macquariensis*	1.2	http://fishbase.org
Catarina pupfish	*Megupsilon aporus*	1.7	http://fishbase.org
Scheel's lampeye	*Micropanchax scheeli*	1.0	http://fishbase.org
Boji Plains nothobranch	*Nothobranchius bojiensis*	1.1	http://fishbase.org
-	*Nothobranchius eggersi*	2.2	http://fishbase.org
Elongate nothobranch	*Nothobranchius elongatus*	1.6	http://fishbase.org
-	*Nothobranchius foerschi*	2.0	http://fishbase.org
Turquoise killifish	*Nothobranchius furzeri*	1.2	http://fishbase.org
-	*Nothobranchius fuscotaeniatus*	1.5	http://fishbase.org
Redfin notho	*Nothobranchius kirki*	1.6	http://fishbase.org
Striped nothobranch	*Nothobranchius taeniopygus*	1.3	http://fishbase.org
Togo Killifish	*Nothobranchius thierryi*	1.4	http://fishbase.org
Uganda nothobranch	*Nothobranchius ugandensis*	1.4	http://fishbase.org
-	*Oryzias curvinotus*	1.1	http://fishbase.org
Javanese ricefish	*Oryzias javanicus*	0.9	http://fishbase.org
-	*Oryzias mekongensis*	0.6	http://fishbase.org

-	*Oxynoemacheilus insignis*	1.0	http://fishbase.org
Powder-blue panchax	*Pachypanchax omalonotus*	1.2	http://fishbase.org
-	*Pachypanchax sakaramyi*	1.6	http://fishbase.org
Eastcoast lampeye	*Pantanodon stuhlmanni*	1.2	http://fishbase.org
Cardinal tetra	*Paracheirodon axelrodi*	2.3	http://fishbase.org
Dusky millions fish	*Phalloceros caudimaculatus*	1.0	http://fishbase.org
Ruwenzori lampeye	*Platypanchax modestus*	1.5	http://fishbase.org
Catemaco molly	*Poecilia catemaconis*	1.8	http://fishbase.org
Amazon molly	*Poecilia formosa*	1.4	http://fishbase.org
Broadspotted molly	*Poecilia latipunctata*	1.7	http://fishbase.org
Shortfin molly	*Poecilia mexicana*	1.0	http://fishbase.org
Guppy	*Poecilia reticulata*	0.8	http://fishbase.org
Sail-fin molly	*Poecilia velifera*	1.7	http://fishbase.org
-	*Poropuntius kontumensis*	1.7	http://fishbase.org
-	*Poropuntius laoensis*	1.2	http://fishbase.org
Isthmian priapella	*Priapella intermedia*	1.3	http://fishbase.org
Bluegreen lampeye	*Procatopus aberrans*	0.8	http://fishbase.org
Variable lampeye	*Procatopus similis*	1.0	http://fishbase.org
Barred topminnow	*Quintana atrizona*	1.5	http://fishbase.org
Mt. Nimba lampeye	*Rhexipanchax nimbaensis*	1.3	http://fishbase.org
Lake minnow	*Rhynchocypris percnurus*	1.6	http://fishbase.org
Adriatic trout	*Salmo obtusirostris*	2.2	http://fishbase.org
Lake trout	*Salvelinus namaycush*	2.1	http://fishbase.org
Freshwater sardinella	*Sardinella tawilis*	1.2	http://fishbase.org
Kindia killi	*Scriptaphyosemion cauveti*	0.7	http://fishbase.org
-	*Scriptaphyosemion schmitti*	1.3	http://fishbase.org
Spanish pupfish	*Spanish toothcarp*	1.6	http://fishbase.org
Bordallo	*Squalius carolitertii*	2.6	http://fishbase.org
Peacock gudgeon	*Tateurndina ocellicauda*	1.3	http://fishbase.org
Valencia toothcarp	*Valencia hispanica*	1.4	http://fishbase.org
Green swordtail	*Xiphophorus hellerii*	1.2	http://fishbase.org

Table. S3 Aspect ratio data of highly migratory marine fish

Common Name	***Species***	**AR**	**Ref**
Slender tuna	*Allothunnus fallai*	5.6	http://fishbase.org
Bigeye thresher	*Alopias superciliosus*	2.5	http://fishbase.org
Thresher	*Alopias vulpinus*	1.8	http://fishbase.org

Frigate tuna	*Auxis brachydorax*	6.6	http://fishbase.org
Bullet tuna	*Auxis rochei*	5.5	http://fishbase.org
Frigate tuna	*Auxis thazard*	5.8	http://fishbase.org
Silky shark	*Carcharhinus falciformis*	2.0	http://fishbase.org
Great white shark	*Carcharodon carcharias*	3.5	http://fishbase.org
Portuguese dogfish	*Centroscymnus coelolepis*	1.5	http://fishbase.org
Basking shark	*Cetorhinus maximus*	3.2	http://fishbase.org
Leaping z	*Cybiosarda elegans*	5.6	http://fishbase.org
Kawakawa	*Euthynnus affinis*	5.6	http://fishbase.org
Little tunny	*Euthynnus alletteratus*	4.2	http://fishbase.org
Black skipjack	*Euthynnus lineatus*	4.1	http://fishbase.org
Dogtooth tuna	*Gymnosarda unicolor*	5.7	http://fishbase.org
Black marlin	*Istiompax indica*	6.8	http://fishbase.org
Atlantic sailfish	*Istiophorus albicans*	8.5	http://fishbase.org
Indo-Pacific sailfish	*Istiophorus platypterus*	5.9	http://fishbase.org
Atlantic white marlin	*Kajikia albida*	7.4	http://fishbase.org
Striped marlin	*Kajikia audax*	7.1	http://fishbase.org
Skipjack tuna	*Katsuwonus pelamis*	6.5	http://fishbase.org
Escolar	*Lepidocybium flavobrunneum*	5.3	http://fishbase.org
Indo-Pacific blue marlin	*Makaira mazara*	7.7	http://fishbase.org
Blue marlin	*Makaira nigricans*	7.8	http://fishbase.org
White trevally	*Pseudocaranx dentex*	4.4	http://fishbase.org
Eastern Pacific bonito	*Sarda chiliensis*	4.9	http://fishbase.org
Pacific bonito	*Sarda lineolata*	3.7	http://fishbase.org
Striped bonito	*Sarda orientalis*	3.9	http://fishbase.org
Atlantic bonito	*Sarda sarda*	5.8	http://fishbase.org
Shortbill spearfish	*Tetrapturus angustirostris*	6.6	http://fishbase.org
Mediterranean spearfish	*Tetrapturus belone*	7.1	http://fishbase.org
Roundscale spearfish	*Tetrapturus georgii*	5.5	http://fishbase.org
Longbill spearfish	*Tetrapturus pfluegeri*	6.4	http://fishbase.org
Albacore	*Thunnus alalunga*	5.6	http://fishbase.org
Yellowfin tuna	*Thunnus albacares*	6.0	http://fishbase.org
Blackfin tuna	*Thunnus atlanticus*	5.8	http://fishbase.org
Southern bluefin tuna	*Thunnus maccoyii*	7.8	http://fishbase.org
Bigeye tuna	*Thunnus obesus*	6.8	http://fishbase.org
Pacific bluefin tuna	*Thunnus orientalis*	6.3	http://fishbase.org
Atlantic bluefin tuna	*Thunnus thynnus*	6.3	http://fishbase.org
Longtail tuna	*Thunnus tonggol*	7.2	http://fishbase.org

Swordfish	*Xiphias gladius*	7.1	http://fishbase.org